Supplementary Material: Unraveling Aqueous Alcohol Freezing: new theoretical tools from graph theory to extract molecular processes in MD simulations

Rawan AbouHaidar,[a] Sana Bougueroua,[b] Denis Duflot,[a] Marie-Pierre Gaigeot,[b] Barbara Wyslouzil,[c] and Céline Toubin,*[a]

List of tables and figures

[a] *Univ. Lille, CNRS, UMR 8523 — PhLAM Physique des Lasers Atomes et Molécules, F-59000 Lille.*
[b] *Université Paris-Saclay, Univ Evry, CY Cergy Paris Université, CNRS, LAMBE, 91025 Evry-Courcouronnes, France.*
[c] *William G. Lowrie Department of Chemical and Biomolecular Engineering, Department of Chemistry and Biochemistry, Ohio State University, Columbus, Ohio, USA.*
-; Tel: +3 33 20 43 43 80; E-mail: celine.toubin@univ-lille.fr

In this paper, classical Molecular Dynamics (MD) simulations explore the temperature-dependent behavior of 1-pentanol (linear alcohol) and 3-hexanol (branched alcohol) films covering the air-water interface. Table S1 summarizes key properties of n-alcohol isomers of pentanol and hexanol. The data reflects the higher solubility and larger molecular footprint of the branched isomers compared to the straight-chain ones. Additionally, the molecular areas for 1-pentanol and 3-hexanol were used to estimate the number of alcohol molecules required to form a monolayer on the water surface.

Table S1 Key properties reported for n-alcohol isomers: Gibbs free energies of adsorption (ΔG_{Ads}) in kJ/mol, molecular areas at monolayer coverage (A_{ML}) in Å^2, and surface concentrations at monolayer coverage (c_{ML}) in molecules/cm^2.

Alcohol	Length[a] (Å)	ΔG_{Ads}[a] (kJ/mol)	A_{ML}[a] (Å^2)	c_{ML}[a] (molecules/cm^2)	Solubility[c] (mole fraction)	Surface tension[d] (mN/m)
1-Pentanol	6.0	-17.0 $\pm$ 0.5	41 $\pm$ 2	3.3×10^{14}	0.0054	26.2
1-Hexanol	6.5	-19.2 $\pm$ 1.5	44 $\pm$ 2	3.1×10^{14}	0.0013	27.0
3-Pentanol	4.0	-16.7 $\pm$ 0.3	63 $\pm$ 2	2.2×10^{14}	0.0151	26.0
3-Hexanol	4.5	-19.1 $\pm$ 0.6	60 $\pm$ 2	2.2×10^{14}	0.0035	25.4

a 1

b 2

c 3, solubility in water at 283 K

d 4 and 5, respectively, surface tension of pure alcohol compounds at 283 K

1 Molecular Dynamics Trajectories

1.1 Surface tension

The surface tension γ (mN/m) was calculated at 10 ns intervals along the MD trajectories (Figure S1). The cumulative average surface tension[6,7], along with its corresponding errors, was then computed.

Table S2 presents the surface tension values for the last 50 ns and their associated errors. The increasing standard deviation with decreasing temperature indicates greater fluctuations in surface tension throughout the simulation. Our analysis assumes that a standard deviation higher than 10 mN/m indicates that the system has not reached equilibrium at that specific temperature. Consequently, such temperature will not be considered in further analysis. Figure S1a and Table S2 display the surface tension over the 150 ns period at different temperatures. As the temperature decreases, fluctuations in surface tension become more pronounced, with significant variations observed at 192 K. The rise in standard deviation at lower temperatures highlights these significant fluctuations and oscillations in the surface tension.

Thus, stable surface tension values were achieved at higher temperatures (283 K to 206 K). However, at 192 K, extending the simulation duration may be necessary to achieve convergence, as 150 ns is not sufficiently long to provide accurate values. The accumulated average surface tension and the Root Mean Square (RMS) of the errors have been calculated at each temperature (Figure S2).

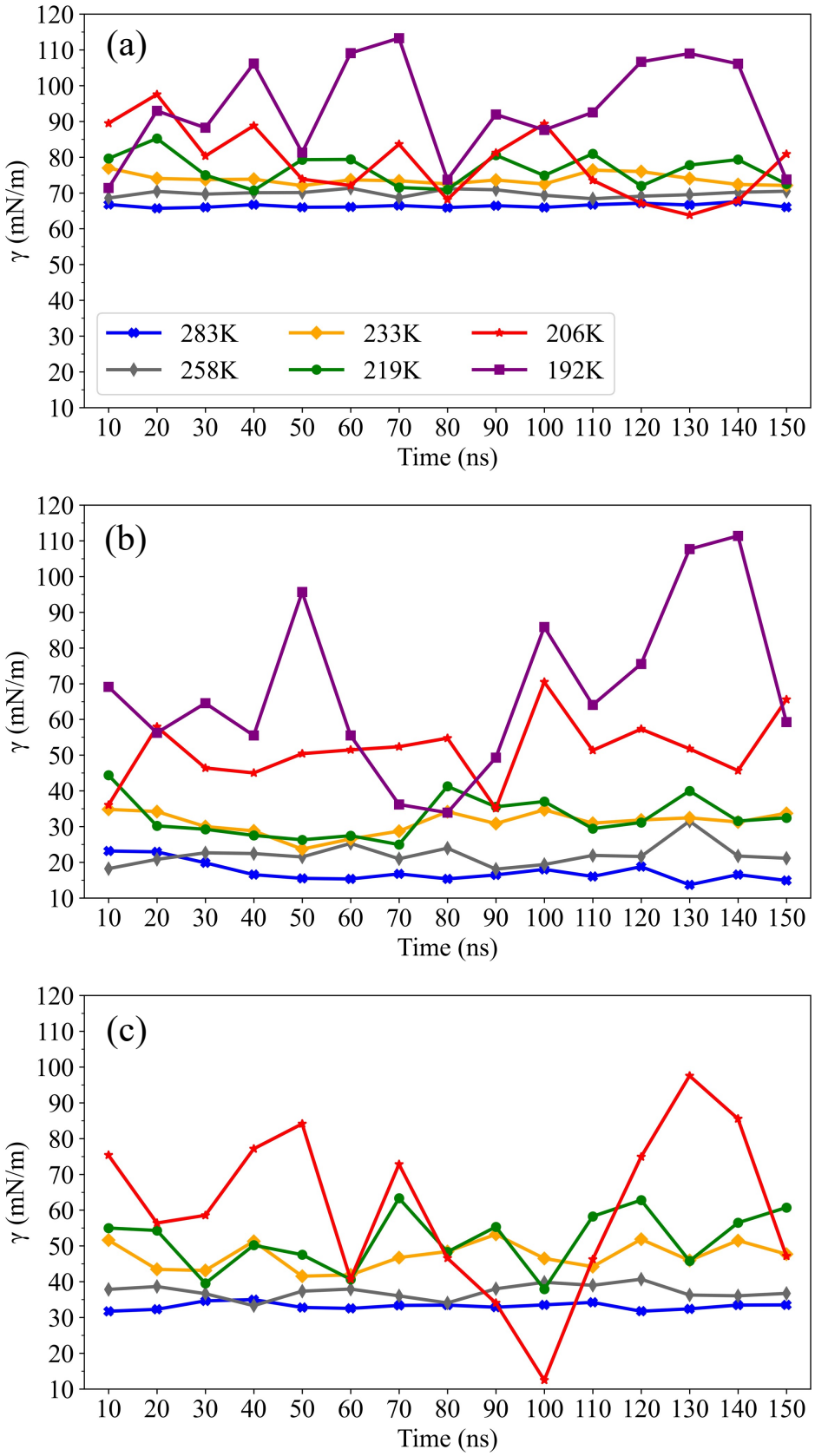

Fig. S1 Cumulative averaged surface tension γ (mN/m) for each temperature for (a) pure water solution, (b) 1-pentanol monolayer, and (c) 3-hexanol monolayer on an aqueous solution.

Table S2 Surface tension values (mN/m) for the last 50 ns of the simulation, along with their associated errors, for the TIP4P/2005 water model at various temperatures.

Time (ns) \ T (K)	283	258	233	219	206	192
100-110	66.71 ± 0.70	68.36 ± 1.20	76.37 ± 1.95	80.97 ± 1.35	73.55 ± 9.00	92.52 ± 3.15
110-120	67.14 ± 0.80	69.10 ± 0.85	75.99 ± 1.65	71.96 ± 5.00	67.14 ± 6.50	106.64 ± 3.55
120-130	66.63 ± 0.55	69.52 ± 0.75	74.05 ± 2.55	77.78 ± 1.95	63.81 ± 10.50	108.98 ± 4.95
130-140	67.59 ± 0.75	70.19 ± 0.55	72.37 ± 1.80	79.33 ± 5.50	67.83 ± 7.00	106.10 ± 3.75
140-150	66.05 ± 0.29	70.48 ± 1.15	72.10 ± 2.10	72.50 ± 2.25	80.86 ± 6.00	73.76 ± 10.50
Standard deviation	0.58	0.84	1.98	4.07	6.70	14.81
Average	66.82 ± 0.64	69.53 ± 0.93	74.18 ± 2.03	76.51 ± 3.63	70.64 ± 7.98	—

To compare our simulations accurately, we utilized the fitting parameters obtained from Vega and de Miguel to calculate the surface tension of the TIP4P/2005 water model at various temperatures (Figure S2).

$$\gamma = c_1 \left(1 - \frac{T}{T_c}\right)^{\frac{11}{9}} - c_2 \left(1 - \frac{T}{T_c}\right)^{6}$$

On average, we found that the simulated surface tension of pure water was approximately 5 mN/m lower than the values derived from Vega and de Miguel equation. At 298 K, our calculated surface tension is 64.3 ± 0.6 mN/m, which closely aligns with computational values of the TIP4P/2005 water model of 65.4 mN/m (without including long-range corrections)[8], 69.3 ± 0.9 mN/m (including long-range corrections)[8] and 68.4 ± 1.1 mN/m[9] as well as the experimental value of 71.7 mN/m[8]. Thus, this discrepancy can be attributed to the absence of the tail correction to the surface tension in our simulations, caused by the truncation of the Lennard-Jones potential, which would increase the surface tension by at least 2 mN/m[8,9]. On the other hand, as the temperature decreases, the kinetic energy of the liquid's molecules also decreases. Consequently, the molecules exhibit slower movement and stronger intermolecular forces at the surface, leading to an increase in surface tension.

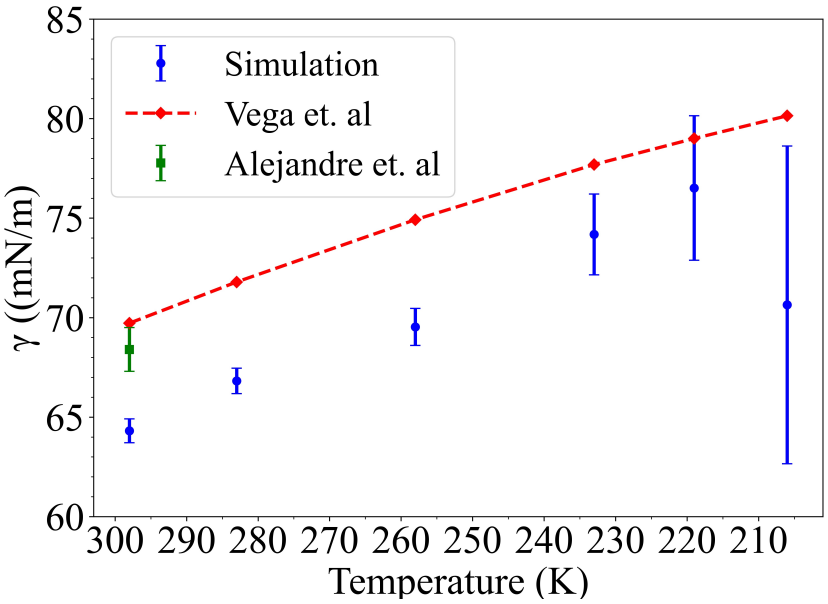

Fig. S2 Comparison of surface tension values for pure water solution (TIP4P/2005 model) obtained from (blue) our simulations, (red) equation from[8], and (green)[9] at different temperatures. The fitting parameters for the surface tension equation of the TIP4P/2005 model are: c_1 = 227.86 mN/m, c_2 = 0.6413 (dimensionless), and the critical temperature T_c = 641.4 K[8].

The surface tension was calculated over time for each temperature for both 1-pentanol and 3-hexanol solutions (Figure S1b and c). For 1-pentanol solutions, temperatures above 206 K show stabilized surface tension, with multiple simulation runs converging to similar results with low standard deviations. However, at 192 K, significant fluctuations

persisted even after extending the simulation to 200 ns, indicating that equilibrium was not reached (Table S3). For 3-hexanol solutions, convergence was observed at temperatures above 219 K, with stable surface tension values over time. At 206 K, large fluctuations were still observed at 200 ns (Table S4).

Table S3 Surface tension values (mN/m) for the last 50 ns of the simulation, along with their associated errors, for a 1-pentanol monolayer on an aqueous water slab at various temperatures.

T (K) / Time (ns)	283	258	233	219	206	192
100-110	16.03 ± 1.65	21.92 ± 1.85	30.96 ± 2.80	29.42 ± 2.65	51.32 ± 11.50	64.04 ± 7.50
110-120	18.77 ± 0.85	21.62 ± 1.20	31.84 ± 1.35	31.14 ± 5.50	57.29 ± 10.50	75.53 ± 6.00
120-130	13.69 ± 0.70	31.52 ± 5.50	32.45 ± 3.15	39.98 ± 2.35	51.76 ± 6.50	107.64 ± 3.40
130-140	16.55 ± 0.70	21.75 ± 2.70	31.28 ± 1.50	31.55 ± 9.00	45.65 ± 6.50	111.37 ± 7.00
140-150	14.90 ± 1.40	21.12 ± 1.30	33.72 ± 2.55	32.46 ± 4.95	65.55 ± 10.00	59.23 ± 3.80
Standard deviation	1.91	4.45	1.10	4.10	7.51	24.45
Average	15.99 ± 1.13	23.59 ± 2.97	32.05 ± 2.38	32.91 ± 5.45	54.32 ± 9.24	—

Table S4 Surface tension values (mN/m) for the last 50 ns of the simulation, along with their associated errors, for a 3-hexanol monolayer on an aqueous water slab at various temperatures.

T (K) / Time (ns)	283	258	233	219	206
100-110	34.21 ± 1.25	38.99 ± 1.45	44.20 ± 2.45	58.25 ± 7.00	46.21 ± 5.50
110-120	31.74 ± 1.10	40.68 ± 1.50	51.84 ± 3.20	62.79 ± 11.00	74.89 ± 6.50
120-130	32.40 ± 1.55	36.26 ± 0.85	45.92 ± 1.10	47.78 ± 9.00	97.53 ± 7.50
130-140	33.46 ± 1.40	36.05 ± 1.05	51.50 ± 3.10	56.46 ± 6.50	85.53 ± 11.00
140-150	33.50 ± 0.90	36.72 ± 1.40	47.69 ± 2.80	60.72 ± 9.50	47.17 ± 5.50
Standard deviation	0.98	2.02	3.38	6.61	22.97
Average	33.06 ± 1.26	37.74 ± 1.28	48.23 ± 2.64	56.80 ± 8.76	—

1.2 Density probability distribution

The density distribution profiles were computed for water oxygen, the carbon linked to the OH group (C_{OH}), and the terminal carbons (CT) for 1-pentanol and 3-hexanol at different temperatures (Figure S3).

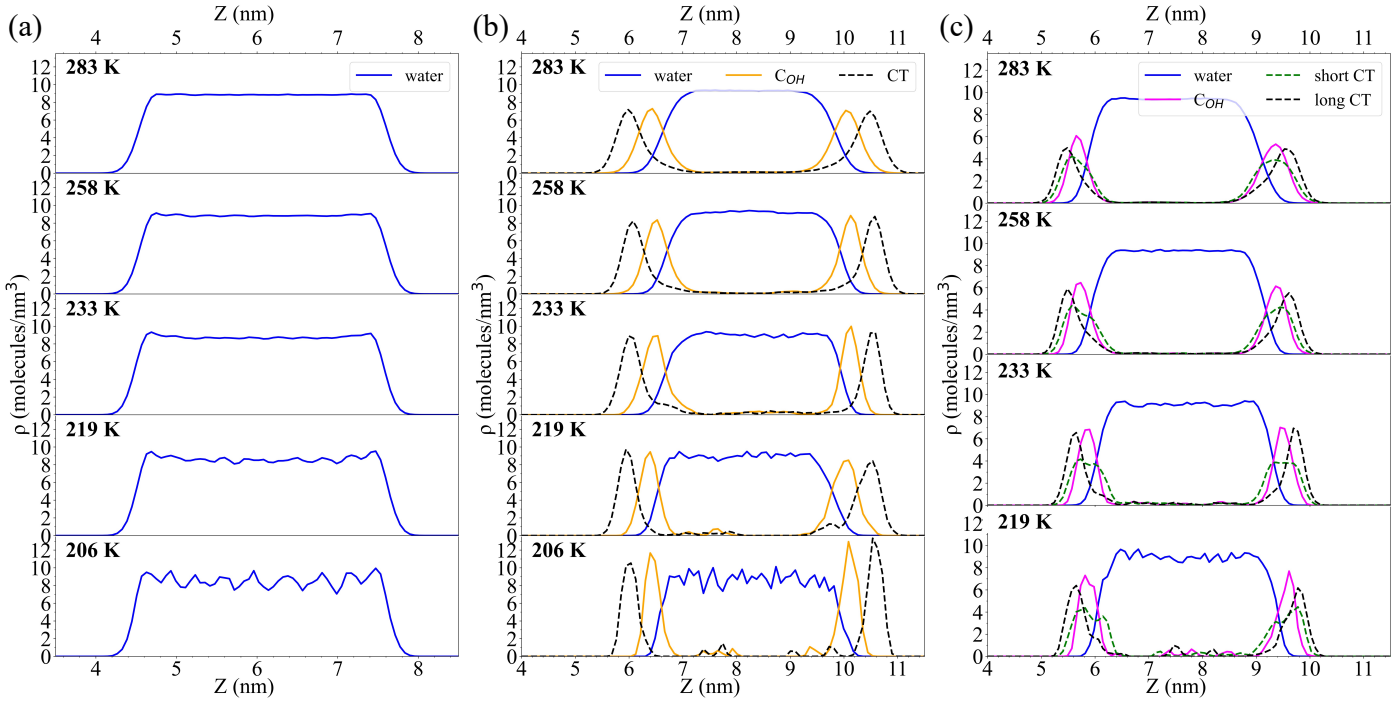

Fig. S3 Density distribution profiles of water oxygen, C_{OH} group, and terminal carbons (CT) for (a) TIP4P/2005 water model, (b) 1-pentanol, and (c) 3-hexanol solutions at different temperatures during the last 10 ns of a 150 ns simulation. The density was calculated based on the number of molecules per cubic nanometer using 200 slices.

1.3 Angular distributions

To investigate the orientation of alcohol molecules at the interface, we introduce an orientation parameter, $\cos(\theta)$, where θ represents the average angle between the vector of the carbon linked to the hydroxyl headgroup (C_{OH}) and the long terminal carbon (CT) relative to the normal vector of the water surface (the z-direction of the computational box). In this context, the alcohol molecule will be perpendicular to the surface plane when $\theta = 0°$ and parallel to the surface plane when $\theta = 90°$ (Figure S4).

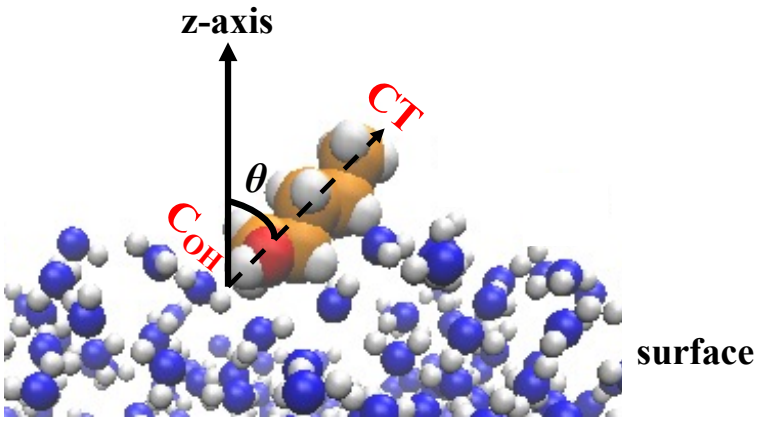

Fig. S4 Schematic representation of the angle θ.

An optimized gas phase TraPPE-UA model shows that 1-pentanol and 3-hexanol molecules have distances of 5.1 Å and 3.9 Å, respectively, between the long CT and the C_{OH} atoms. Additionally, by analyzing the half-maximum width of the density distributions (Figure S3), we can determine the thickness of the CT and C_{OH} atoms monolayer at the surface, representing the average distance between the CT and the C–OH atom. This calculation enables us to estimate the average

angle θ at various temperatures, as the projection of the distance to the z-axis, as detailed in Table S5.

Table S5 Average angle (θ) formed between the alcohol chain (C_{OH} – CT axis), noted as $D_{C_{OH}--CT}$, and the normal to the surface (z-axis).

T (K)	1-pentanol		3-hexanol	
	$D_{C_{OH}--CT}$ (Å)	θ (°)	$D_{C_{OH}--CT}$ (Å)	θ (°)
283	3.60 – 4.50	45° – 28°	1.65 – 2.45	65° – 51°
258	4.50	28°	1.65 – 2.45	65° – 51°
233	3.60 – 4.50	45° – 28°	2.45	51°
219	4.50	28°	1.65	65°
206	4.50	28°	—	—

A comparative analysis of 1-pentanol and 3-hexanol orientations at the surface reveals distinct patterns. 1-pentanol molecules tend to align more parallel to the surface normal, with angles ranging between 28° and 45° to the z-axis at higher temperatures, influenced by their dynamic behavior at the surface. Conversely, the angular distribution for 3-hexanol is less distinct and closer to the surface plane, suggesting a higher probability of residing close to the surface plane rather than aligning parallel to the z-axis. This difference presumably takes a route from the linear structure and longer chain length of 1-pentanol (C_5) compared to the branched structure of 3-hexanol with its shorter chain length (C_3 or C_2). Ekholm *et al.* mentioned that with increasing hydrocarbon tail length, the orientation of the molecules becomes more pronounced with the hydrophobic tails aligning more consistently with the surface normal and the hydroxyl groups pointing toward the water. In summary, 1-pentanol tends to be more perpendicular to the surface, while 3-hexanol tends to be more parallel, with angles below and above 50°, respectively.

According to Walz et al.[10], desolvation of alkyl chains and increased van der Waals interactions significantly influence alcohol orientation. Linear alcohols like 1-pentanol exhibit greater desolvation, resulting in a straighter and more perpendicular orientation to the surface plane. In contrast, branched alcohols like 3-pentanol show partial desolvation, keeping the terminal segment closer to the surface due to the short chain length and *gauche* defects. This trend is supported by XPS studies[11], indicating increasing alcohol orientation toward the surface normal with chain length, highlighting the importance of lateral hydrophobic interactions.

The shift in angular distribution also correlates with the differences in surface tension reduction[12], with 1-pentanol's parallel molecular arrangement consistent with a sharp drop in surface tension compared to 3-hexanol.

Furthermore, a minimal effect of temperature on this distribution is likely due to restricted alcohol movement at lower temperatures. Consequently, we observe less variation in the orientation angles.

2 Graph Theory Analysis

Figure S5 presents two examples of 2D-MolGraphs of alcohol films at the aqueous interface within the BIL thickness at 283 K. As can be seen with the directed edges, water oxygen atoms (red) and alcohol oxygen atoms (yellow) are connected by H-bonds. As discussed in the main text, the analysis of the graph reveals that molecules are more connected by H-bonds, with linear chains of 1-pentanol. In contrast, 3-hexanol, being a branched alcohol, shows weaker connectivity and more clustering compared to 1-pentanol. Moreover, these graphs indicate that some alcohol molecules are either free or forming dimers or trimers with water molecules. However, these graphs are instantaneous views of one conformation for each system, highlighting the importance of obtaining statistics along the trajectory to fully capture the connectivity at the interface.

In this study, our focus is on the interface, also known as the Binding Interfacial Layer (BIL)[13]. To achieve a balance between computational efficiency and statistical accuracy, we analyze simulation snapshots at specific intervals. For example, in 10 ns of dynamic data (the last 10 ns of a 150ns simulation), which generates 10,000 snapshots, we find that analyzing every 100 ps equivalent to 100 snapshots provides a sufficient level of detail.

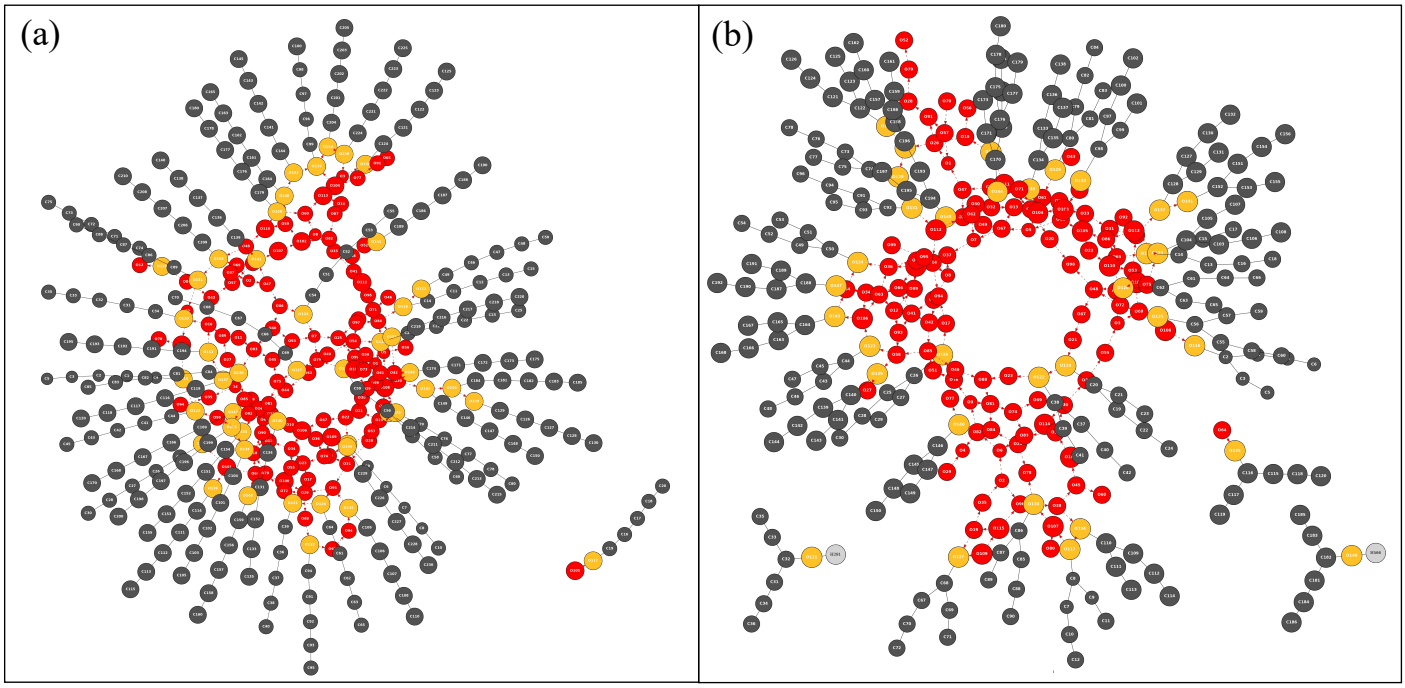

Fig. S5 Example of 2D-MolGraphs of two conformers of alcohol film at the air-water interface at 283 K: (a) 1-pentanol and (b) 3-hexanol. Vertex colors indicate atom types: water oxygen atoms in red, carbon atoms in gray, and alcohol oxygen in yellow. Edges represent bonds: red dashed lines depict hydrogen bonds, arrows show the direction from donor to acceptor, and gray lines represent covalent bonds.

Tables S6, S7, and S8 present the data extracted from the graph analysis of the BIL (Binding Interfacial Layer) at various temperatures for each system: air-water, water with a 1-pentanol film, and water with a 3-hexanol film. Given the dynamic nature of the system, we observe variations in the minimum and maximum number of molecules, with no significant differences in the average total number of atoms across different temperatures. Note that data are given for the upper interface only but similar results are obtained for the outer interface.

Table S6 Characteristics of water molecules in the BIL at the pure air-water interface for different temperatures. The study explores the upper interface of a 6 Å BIL. CC refers to the Connected Component.

Characteristics	283 K	258 K	233 K	219 K	206 K
Number of water molecules					
Average	108	106	105	111	112
Minimum	100	97	94	101	101
Maximum	121	117	114	122	123
Size of the biggest CC (excluding hydrogen atoms)	119	114	113	122	123
Average of the biggest CC (excluding hydrogen atoms)	103	102	103	110	111
Average number of CCs	2	2	1	1	1
Average number of HBs per one water molecule	2	2	3	3	3
Percentage of water molecules incorporated in H-bonded cycles					
Average %	77	82	87	91	92
Minimum %	51	63	66	74	81
Maximum %	92	96	96	100	99
Average number of H-bonded cycles	23	25	30	35	37
Maximum H-bonded cycle size	30	26	25	22	20

Table S7 Characteristics displayed by water and 1-pentanol molecules in the BIL at different temperatures. The study explores the upper interface of a 6.6 Å BIL.

Characteristics	283 K	258 K	233 K	219 K	206 K
Average number of atoms	1116	1105	1171	1214	1161
Number of water molecules					
Average	113	112	114	119	111
Minimum	88	98	101	109	103
Maximum	134	127	123	130	119
Number of 1-pentanol molecules					
Average	43	43	46	48	46
Minimum	39	41	45	46	46
Maximum	46	44	47	48	46
Size of the biggest CC (excluding hydrogen atoms)	391	376	404	413	395
Average of the biggest CC (excluding hydrogen atoms)	350	357	382	397	386
Average number of CCs	4	3	2	2	1
Average of HBs per atom (excluding hydrogen atoms)	1	1	1	1	1
Average percentage of water molecules incorporated in H-bonded cycles	86	89	93	93	95
Average percentage of 1-pentanol molecules incorporated in H-bonded cycles	66	73	78	82	87
Average number of H-bonded cycles	44	47	54	61	55
Maximum H-bonded cycle size	25	24	20	22	21

Table S8 Characteristics displayed by water and 3-hexanol molecules in the BIL at different temperatures. The study explores the upper interface of a 6.6 Å BIL.

Characteristics	283 K	258 K	233 K	219 K
Average number of atoms	958	867	841	808
Number of water molecules				
Average	124	112	107	102
Minimum	111	99	94	87
Maximum	136	125	117	110
Number of 3-hexanol molecules				
Average	33	30	29	28
Minimum	30	29	28	27
Maximum	34	30	29	28
Size of the biggest CC (excluding hydrogen atoms)	361	328	319	306
Average size of the biggest CC (excluding hydrogen atoms)	337	312	305	294
Average number of CCs	3	2	1	1
Average of HBs per atom (excluding hydrogen atoms)	1	1	1	1
Average percentage of water molecules incorporated in H-bonded cycles	87	89	91	92
Average percentage of 3-hexanol molecules incorporated in H-bonded cycles	66	74	81	78
Average number of H-bonded cycles	49	46	46	45
Maximum H-bonded cycle size	26	24	25	23

2.1 Distributions of Connected Components (CCs)

Figure S6a illustrates the statistical distribution of the size of CCs and their numbers across 100 snapshots at different temperatures. At 283 K, a small distribution of CCs of less than 30 atoms is observed, and a main group ranges between 300 to 390 atoms. This indicates that despite the presence of small CCs, atoms still form extended chains and H-bonded networks. However, as the temperature decreases, the disappearance of small CCs is observed as for the pure air-water interface, with a highly pronounced distribution of larger CCs. These larger CCs have a narrow size range, concentrated between 370 and 390 atoms, suggesting that a stronger network is built at lower temperatures. This observation has to be linked with the average number of CCs that decreases upon cooling, reaching almost a single CC (1) at 219 K, as presented in the main text and Table S7.

Similar to the 1-pentanol interface, the shift in Figure S6b as the temperature decreases from 283 K to 219 K reflects an increase in interconnected atoms (oxygens and carbons) through H-bonds, forming a more stable 2D H-bonded network. Hence, similar to the case with 1-pentanol, 3-hexanol molecules also integrate into the 2D H-bonded network in the BIL.

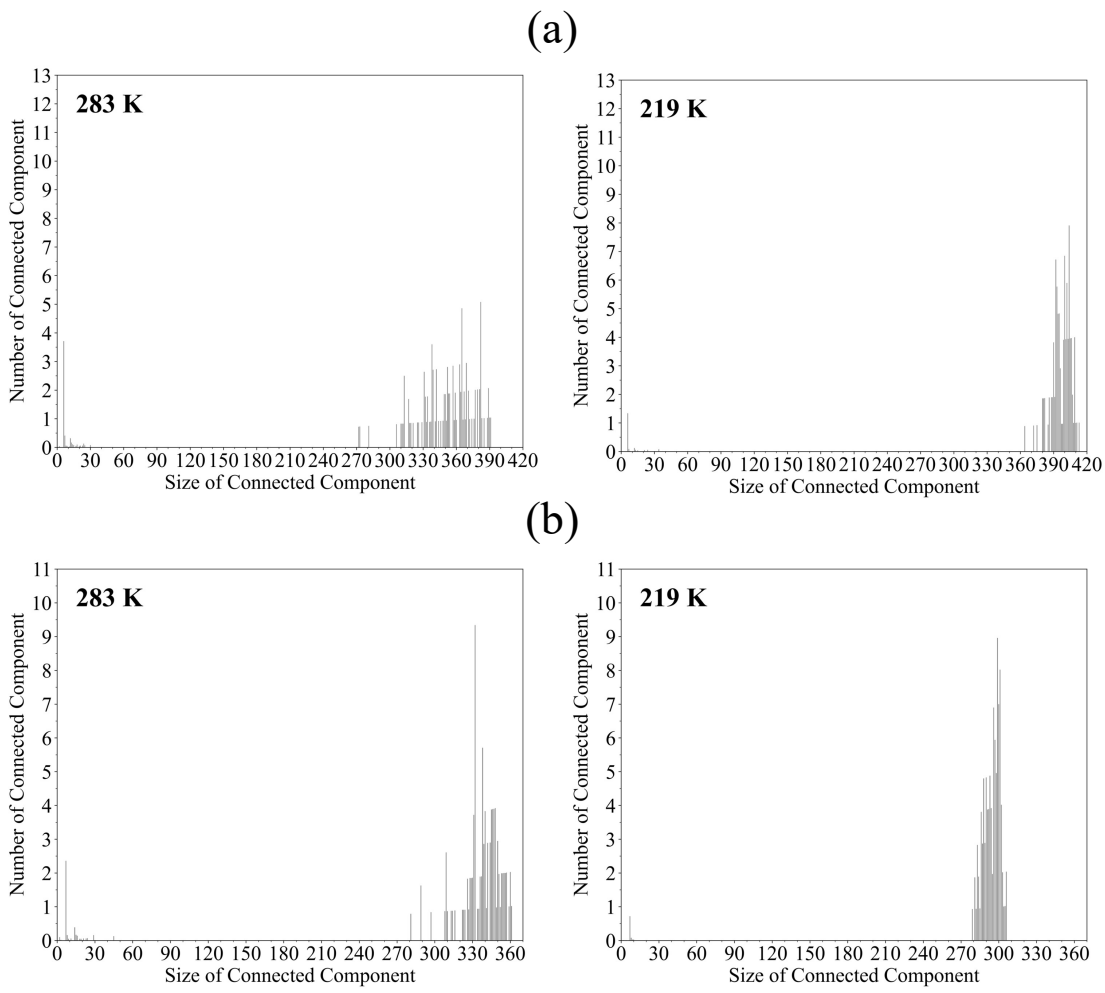

Fig. S6 Connected component (CC) distribution of (a) water and 1-pentanol molecules and (b) water and 3-hexanol molecules at the air-water interface in the presence of 1-pentanol and 3-hexanol films, respectively, at 283 K and 219 K. The study focuses on the upper interface of a 6.6 Å BIL.

2.2 Hydrogen bond distributions

Tables S6, S7, and S8 provide the average number of H-bonds per atom, including HBs formed between water molecules or between water and alcohol molecules (excluding hydrogen atoms) in the BIL. The value is approximately 1, lower

than for the pure air-water interface (from 2 to 3), which can be attributed to the inclusion of carbons from alcohols (1-pentanol or 3-hexanol) into the picture. The fact that this determination includes all atoms, *i.e.*, also surface carbon atoms that may not form H-bonds. These carbon atoms align at the interface and do not form H-bonds, thereby lowering the average number of H-bonds per atom. Therefore, we have calculated the number of H-bonds per atom that belong to the 2D network (Figure S8).

For instance, Figure S7 displays geometries extracted from selected snapshots focusing on specific molecules, to illustrate the different HB formations as well as different counts of HBs between water and 1-pentanol molecules. These configurations range from 1 HB to up to 4 HBs, where water molecules can form a maximum of 4 HBs, while 1-pentanol molecules can form a maximum of 2 HBs. Not that, these snapshots are provided for illustration purposes only and do not represent statistical data. With these snapshots, one can see H-bonds between pentanol with water (Figure S7a and b), direct H-bonds between pentanol molecules (Figure S7b), water molecules H-bonded to both water and pentanol (Figure S7c), just water molecules H-bonded without pentanol (Figure S7d), and finally pentanol molecules mediated by water molecules (Figure S7e).

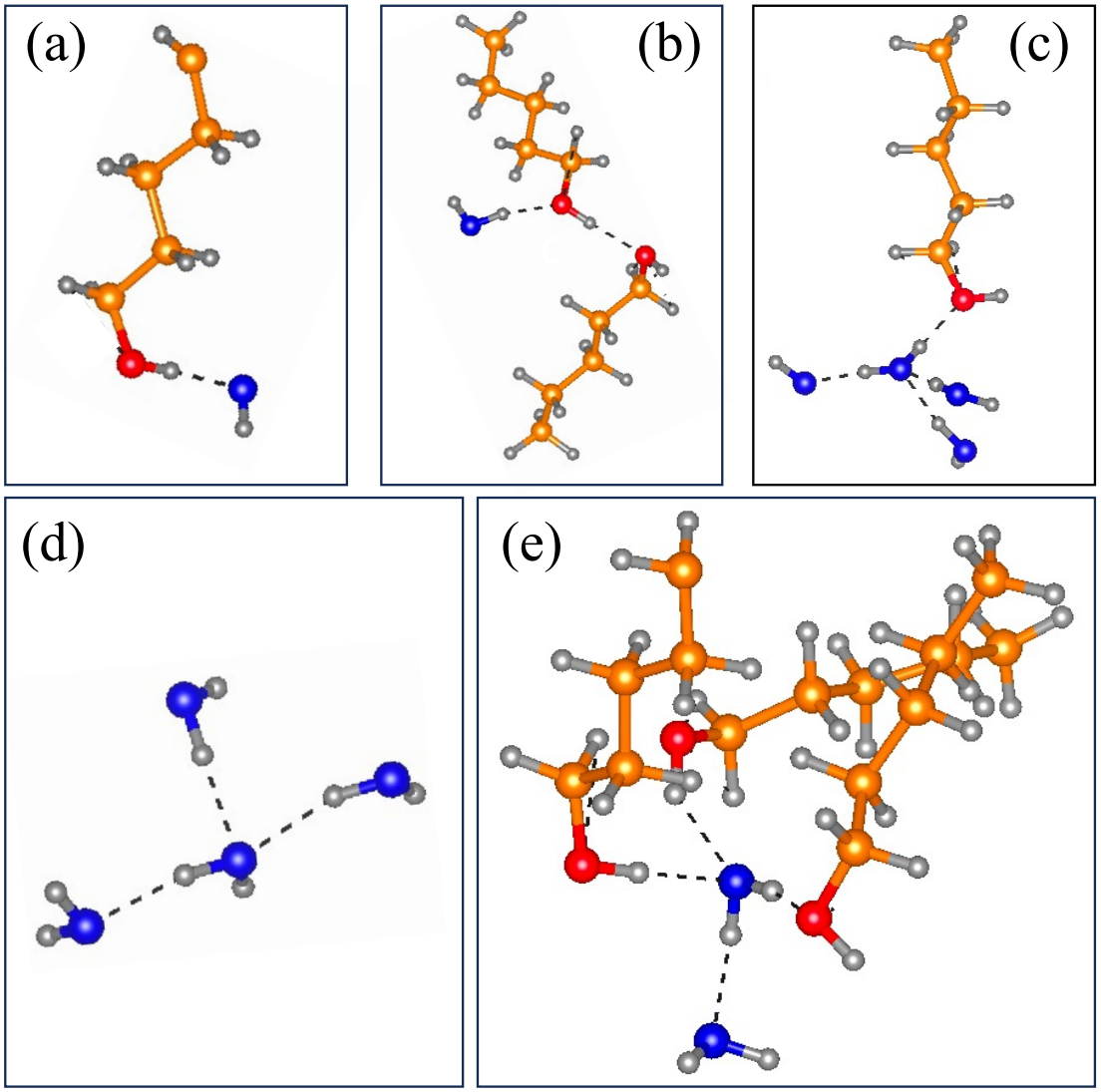

Fig. S7 Geometries extracted from snapshots showing the formation of different types of hydrogen bonds in the case of the 1-pentanol-water interface: a) pentanol-water, b) and c) pentanol-pentanol and pentanol-water d) water-water molecules, d) pentanol-water.

Following this, we examine the time evolution of the number of H-bonds per oxygen atom (water and alcohol) as shown in Figure S8, considering H-bonds ranging from 1 to 4. This latter detailed analysis allows us to understand the H-bonding dynamics in the presence of 1-pentanol at different temperatures. Comparing these distributions at low temperatures to the pure water interface (Figure S8a), we note that for pure water, the highest distribution is for 3 HBs, followed by 2 HBs, with 1 and 4 HBs overlapping at less than 20 atoms. In contrast, for 1-pentanol (Figure S8b), the highest distribution is for 2 HBs, and 3-4 HBs overlapping with also high distribution and well separated from the distribution for 1 HBs. Added up together, configurations with 2,3, and 4 H-bonds involve $\simeq$ 170 atoms, while only $\simeq$ 10 atoms are involved in configurations with just 1 HB, at 219 K. Hence, in the presence of 1-pentanol, a more robust H-bonded network at lower temperatures. Consequently, both 1-pentanol and water molecules tend to predominantly form 2 to 3 HBs, with 2 HBs being the most prevalent configuration.[14] reported that the enhanced tetrahedrality of water observed in alcohol-water solutions arises from the hydrogen bonding of water to the alcohol hydroxyl group.

The hydrogen bonding in the 3-hexanol interface as shown in Figure S8c is less marked than in the 1-pentanol interface with the BIL tending to form 2, 3, and 4 HBs, involving $\approx$ 110 atoms at 219 K. This is fewer than in the 1-pentanol system (170 atoms), but stronger than in the pure water interface, likely due to interactions between the oxygen atoms of the alcohol and water molecules.

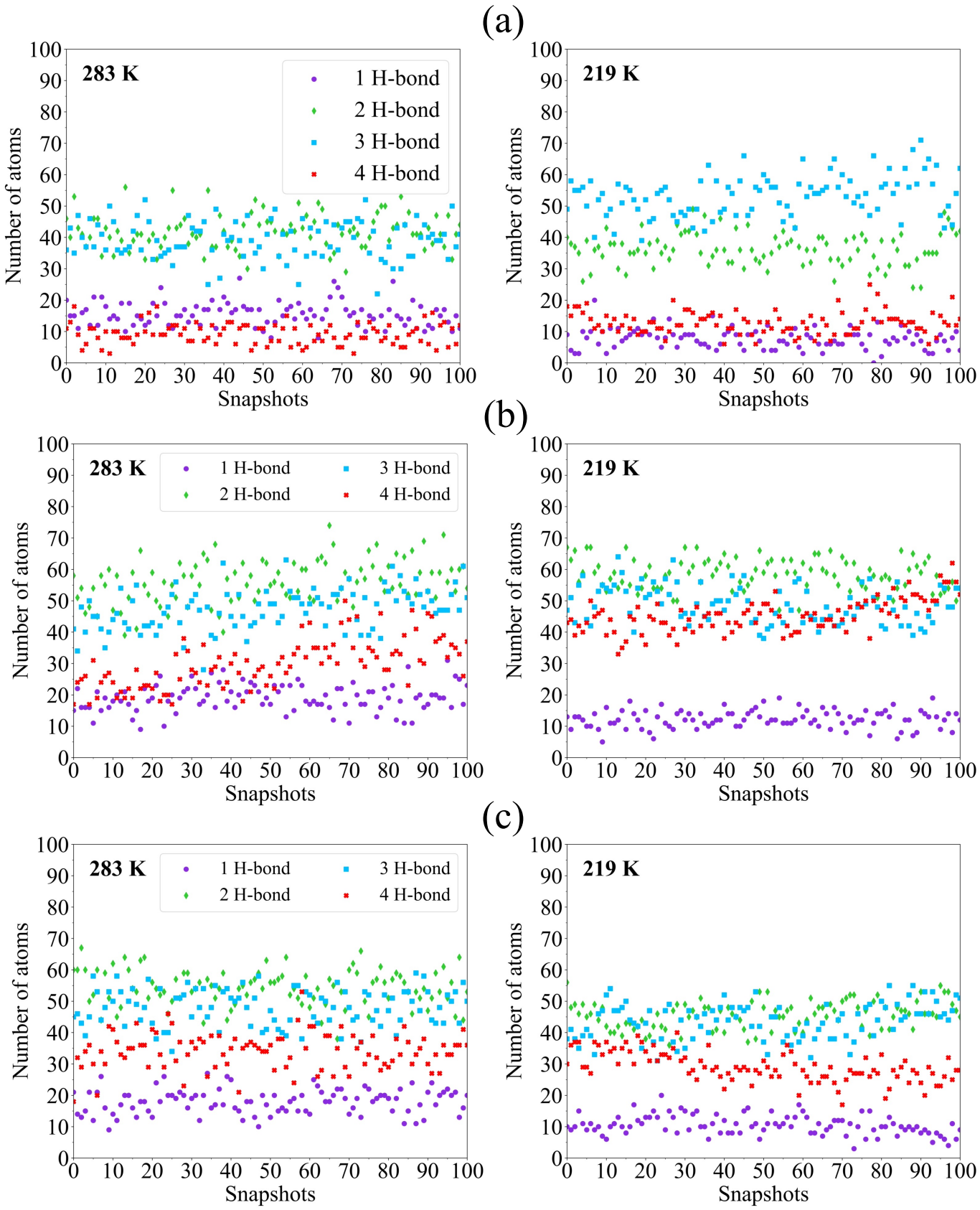

Fig. S8 The evolution of distinct H-bonds between atoms along the 100 snapshots of (a) pure air-water interface and (b) 1-pentanol-water interface and (c) 3-hexanol-water interface, at 283 K and 219 K. The study focuses on the upper interface of a 6.6 Å BIL.

2.3 H-bonded cycle size distributions

To delve deeper into the cycle composition, we analyzed the involvement of 1-pentanol and 3-hexanol in each cycle at the 1-pentanol-water and 3-hexanol-water films, respectively (Figure S9, S10). This analysis helps to determine whether alcohols (1-pentanol and 3-hexanol) are effectively included in the 2DN and in which cycle it prefers to be more involved at various temperatures.

In Figure S9, 1-pentanol is included in various cycles with different ratios, such as 1, 2, or 3 molecules, and varying percentages, with the highest percentage coming from cycles with water and 1-pentanol molecules. As the temperature decreases, the composition variation indicates that in the 5-membered cycles, both configurations comprising 5 water molecules or 4 water + 1 pentanol molecules are found with an almost similar distribution. However, for hexagonal structures, the dominant configuration consists of 5 water molecules + 1 pentanol. Therefore, 1-pentanol plays a significant role in forming the hexagonal cycles, particularly the percentage increased from 11.47% of total 26.90% at 283 K to 22.2% of total 37.15% at 206 K. The increased presence of 1-pentanol in hexagonal cycles indicates its influence in stabilizing and promoting the formation of these "ice-like" structures within the 2D H-bonded network at the BIL.

In Figure S10, we observe the distribution of H-bonded cycle sizes across different temperatures. At 283 K, cycle 5 dominates with a distribution of 38.73%, followed by cycles 4 and 6, each accounting for approximately 22% of occurrences. As the temperature decreases to 219 K, the prevalence of cycle 5 increases to 44%, while the distributions of cycles 4 and 6 remain relatively stable. Examining the composition of each cycle provides further insights. Cycle 5 primarily comprises 5 water molecules without any involvement of 3-hexanol alcohols. Similarly, cycles 4 and 6 consist predominantly of pure water molecules. This suggests that 3-hexanol plays a role in organizing water molecules into cycles, particularly in 5-membered cycles, thereby strengthening the 2D H-bonded network. However, 3-hexanol does not directly participate in the H-bonded cycles, in contrast to our observations with 1-pentanol, where the dominant composition includes pentanol-water cycles rather than pure water alone.

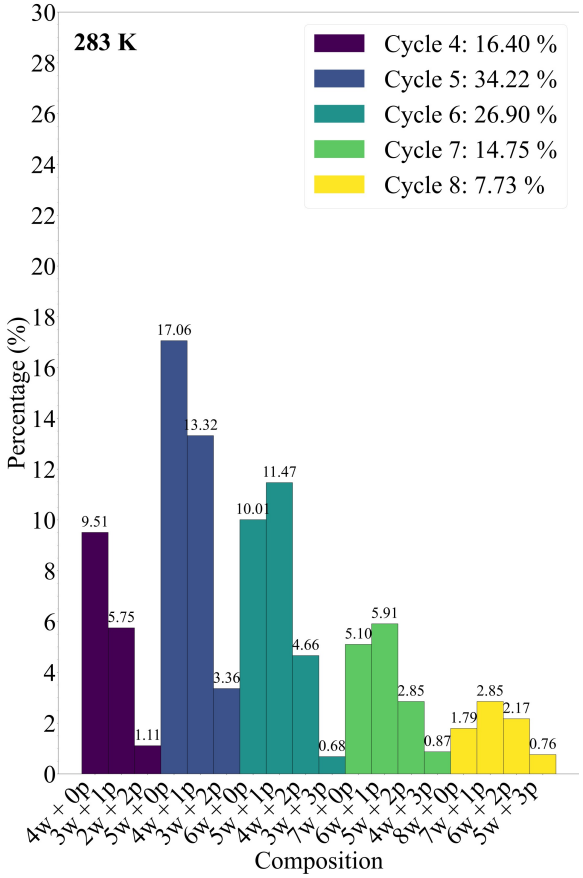
283 K
Cycle 4: 16.40 %
Cycle 5: 34.22 %
Cycle 6: 26.90 %
Cycle 7: 14.75 %
Cycle 8: 7.73 %
Percentage (%)
Composition
4w + 0p
3w + 1p
2w + 2p
5w + 0p
4w + 1p
3w + 2p
6w + 0p
5w + 1p
4w + 2p
3w + 3p
7w + 0p
6w + 1p
5w + 2p
4w + 3p
8w + 0p
7w + 1p
6w + 2p
5w + 3p
9.51
5.75
1.11
17.06
3.32
3.36
10.01
11.47
4.66
0.68
5.10
5.91
2.85
0.87
1.79
2.85
2.17
0.76

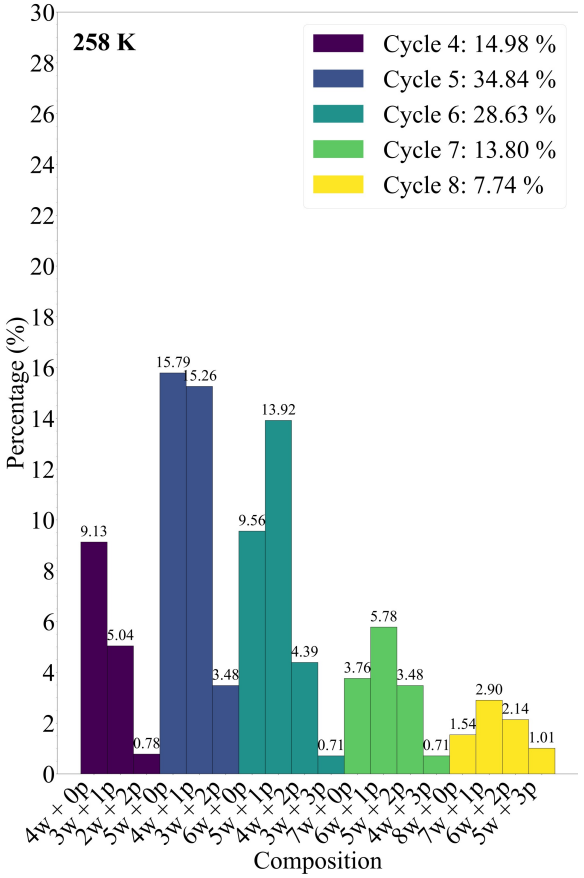
258 K
Cycle 4: 14.98 %
Cycle 5: 34.84 %
Cycle 6: 28.63 %
Cycle 7: 13.80 %
Cycle 8: 7.74 %
Percentage (%)
Composition
4w + 0p
3w + 1p
2w + 2p
5w + 0p
4w + 1p
3w + 2p
6w + 0p
5w + 1p
4w + 2p
3w + 3p
7w + 0p
6w + 1p
5w + 2p
4w + 3p
8w + 0p
7w + 1p
6w + 2p
5w + 3p
9.13
5.04
0.78
15.79
15.26
3.48
9.56
13.92
4.39
0.71
3.76
5.78
3.48
0.71
1.54
2.90
2.14
1.01

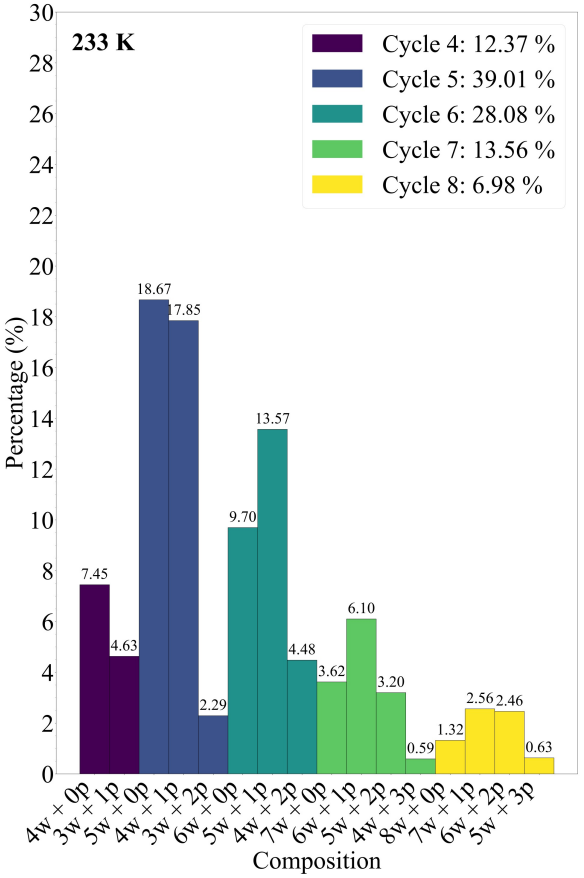
233 K
Cycle 4: 12.37 %
Cycle 5: 39.01 %
Cycle 6: 28.08 %
Cycle 7: 13.56 %
Cycle 8: 6.98 %
Percentage (%)
Composition
4w + 0p
3w + 1p
5w + 0p
4w + 1p
3w + 2p
6w + 0p
5w + 1p
4w + 2p
7w + 0p
6w + 1p
5w + 2p
4w + 3p
8w + 0p
7w + 1p
6w + 2p
5w + 3p
7.45
4.63
18.67
17.85
2.29
9.70
13.57
4.48
3.62
6.10
3.20
0.59
1.32
2.56
2.46
0.63

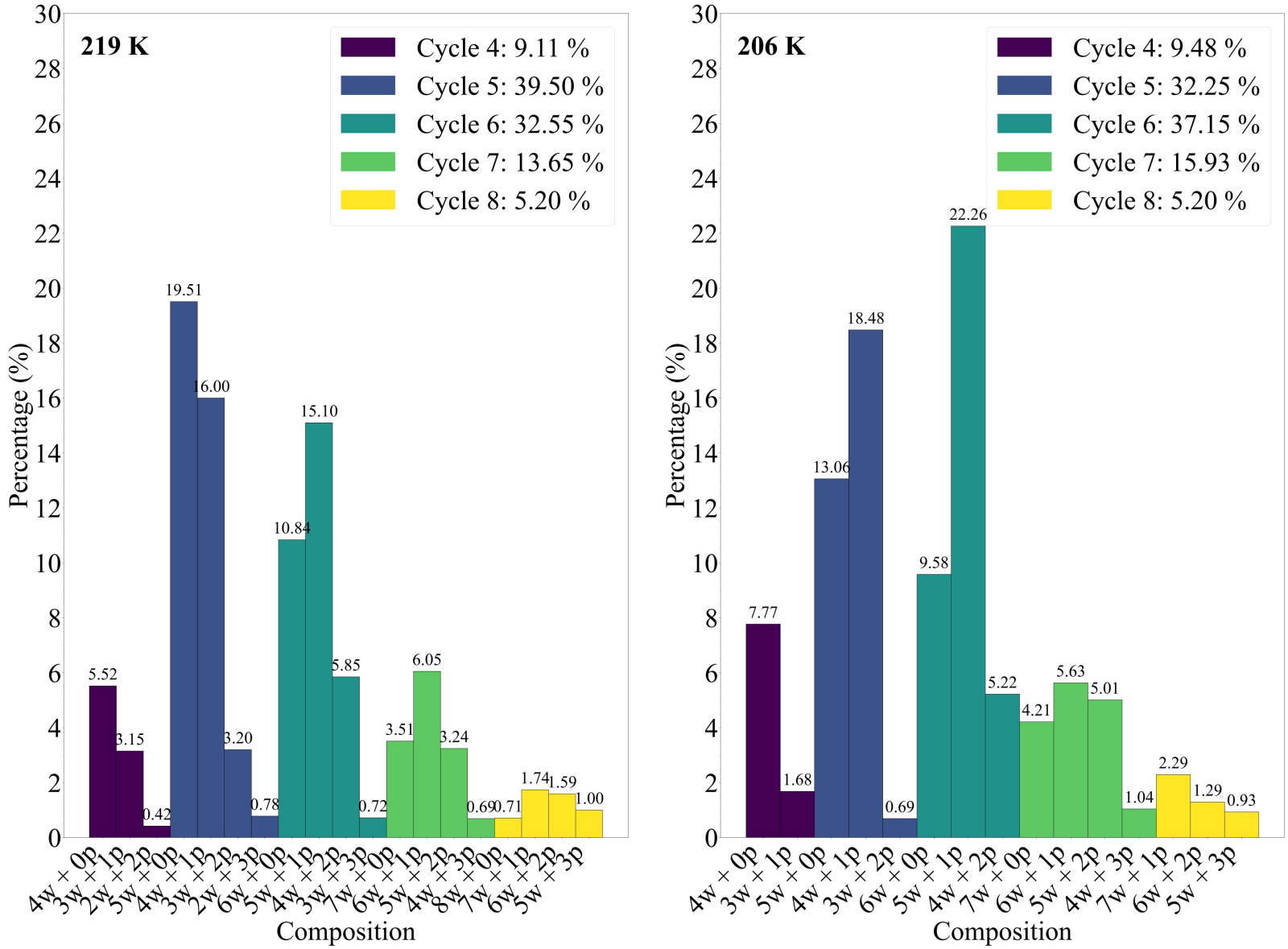

Fig. S9 Distribution of cycles displayed at the air-water interface in the presence of 1-pentanol film at different temperatures (upper interface). The legend denotes the cycle size along with its respective total percentage distribution. The x-axis represents the compositions (water labeled "w" and 1-pentanol labeled "p") contributing to the total percentage of each cycle, while the y-axis denotes the corresponding percentage.

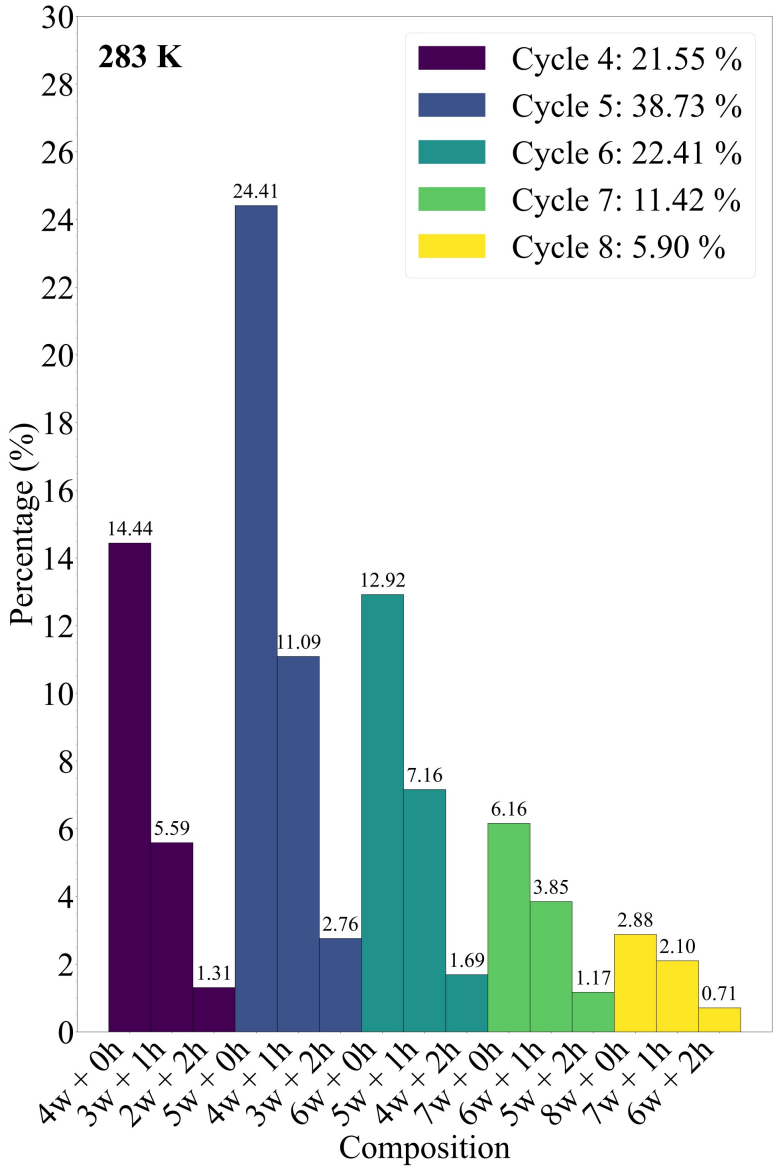
283 K
Cycle 4: 21.55 %
Cycle 5: 38.73 %
Cycle 6: 22.41 %
Cycle 7: 11.42 %
Cycle 8: 5.90 %
Percentage (%)
Composition
4w + 0h
3w + 1h
2w + 2h
5w + 0h
4w + 1h
3w + 2h
6w + 0h
5w + 1h
4w + 2h
7w + 0h
6w + 1h
5w + 2h
8w + 0h
7w + 1h
6w + 2h
14.44
5.59
1.31
24.41
11.09
2.76
12.92
7.16
1.69
6.16
3.85
1.17
2.88
2.10
0.71

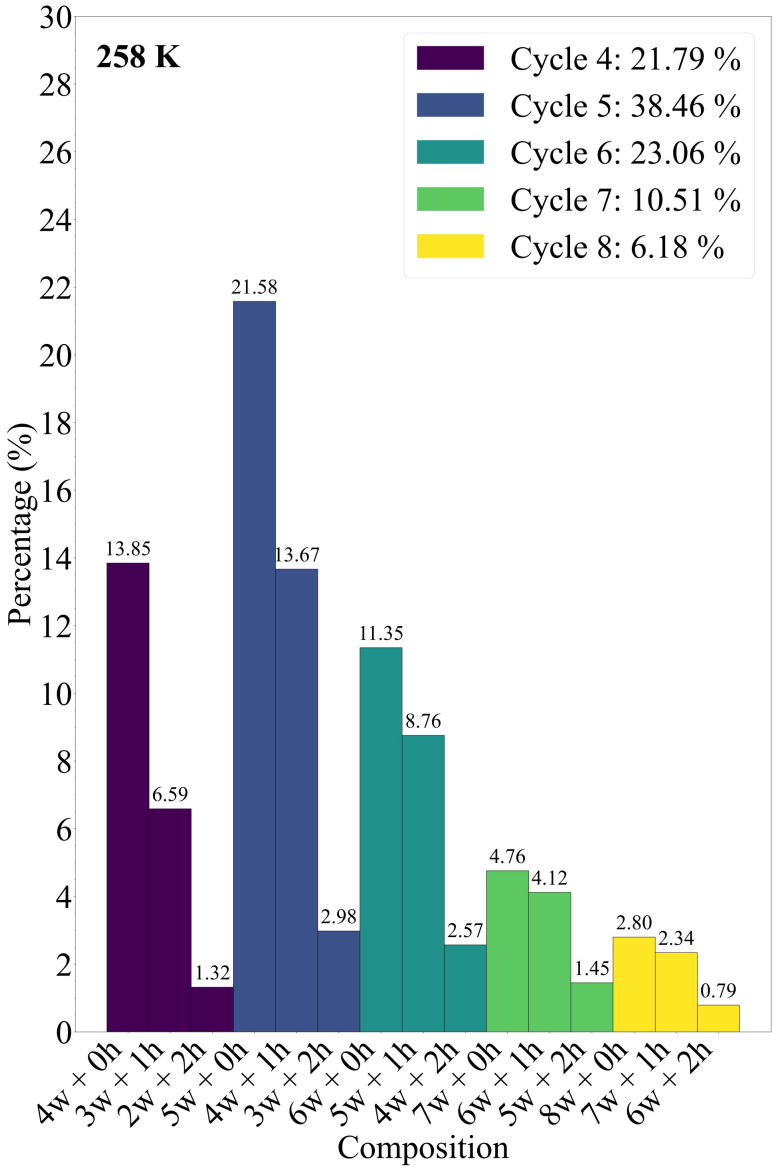
258 K
Cycle 4: 21.79 %
Cycle 5: 38.46 %
Cycle 6: 23.06 %
Cycle 7: 10.51 %
Cycle 8: 6.18 %
Percentage (%)
Composition
4w + 0h
3w + 1h
2w + 2h
5w + 0h
4w + 1h
3w + 2h
6w + 0h
5w + 1h
4w + 2h
7w + 0h
6w + 1h
5w + 2h
8w + 0h
7w + 1h
6w + 2h
13.85
6.59
1.32
21.58
13.67
2.98
11.35
8.76
2.57
4.76
4.12
1.45
2.80
2.34
0.79

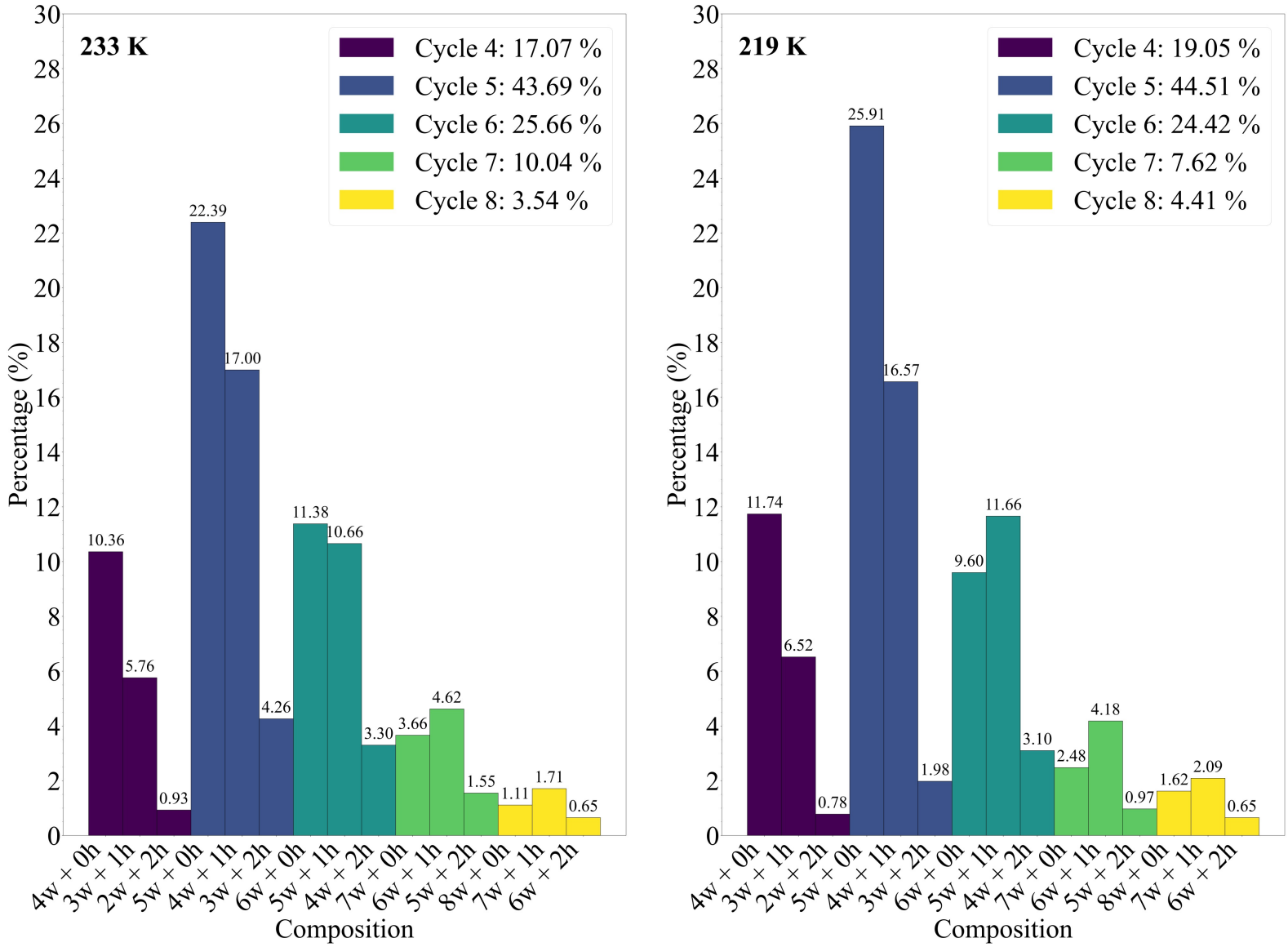

Fig. S10 Distribution of cycles displayed at the air-water interface in the presence of 3-hexanol film at different temperatures (upper interface). The legend denotes the cycle size along with its respective total percentage distribution. The x-axis represents the compositions (water labeled "w" and 3-hexanol labeled "h") contributing to the total percentage of each cycle, while the y-axis denotes the corresponding percentage.

2.3.0.1 Hydrogen bonding interactions

The differences in interactions between the linear and branched alcohol films are evident (Figure S11). 1-pentanol affects more the water-water interactions than 3-hexanol. This can be correlated to the surface tension variations at high temperature. Indeed, it was shown that the significant decrease in surface tension is associated at the molecular level with the preferential adsorption of alcohol molecules at the interface and a reduction in the number of hydrogen bonds between water molecules in the liquid phase[15].

Furthermore, the predominant cycle composition for the 1-pentanol film indicates that alcohol-water interactions are stronger compared to 3-hexanol. Ekholm *et al.* indicated that longer alcohols are immediately oriented as their hydroxyl group can form contact with the water surface. Additionally, both alcohols' oxygen atoms participate in the 2D H-bonded network, forming Ring structures (see Figure 9 in the main text for definition). Consequently, as temperature drops, we observe a decrease in Surfing, Free, and alcohol-alcohol interactions. This is evidenced by the evolution of the connected component from small chains at higher temperatures to a collective and extended 2D H-bonded network.

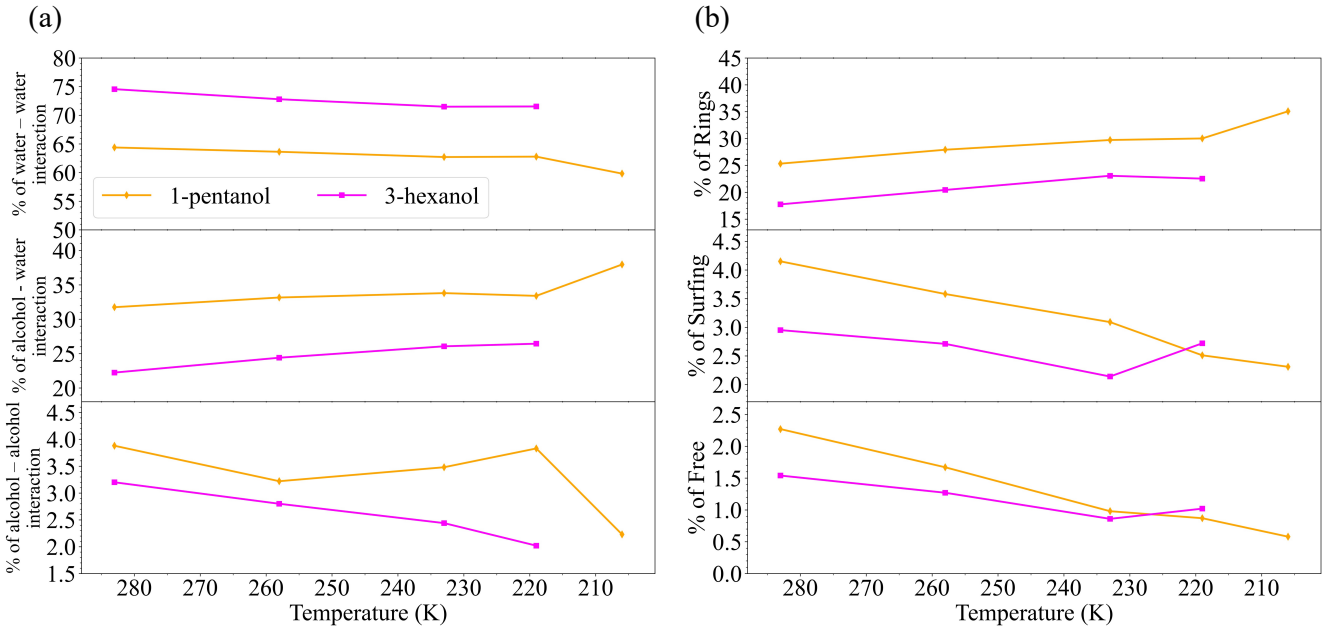

Fig. S11 Distribution of hydrogen bonding interactions in 1-pentanol-water and 3-hexanol-water interface at different temperatures.

Notes and references

1 M.-M. Walz, J. Werner, V. Ekholm, N. L. Prisle, G. Öhrwall and O. Björneholm, *Physical Chemistry Chemical Physics*, 2016, **18**, 6648–6656.

2 V. Ekholm, C. Caleman, J. S. Hub and M. Wohlert, *Physical Chemistry Chemical Physics*, 2021, **23**, 18823–18829.

3 R. Stephenson, J. Stuart and M. Tabak, *Journal of Chemical & Engineering Data*, 1984, **29**, 287–290.

4 A. Mulero, I. Cachadiña and E. L. Sanjuán, *Journal of Physical and Chemical Reference Data*, 2015, **44**, 033104.

5 R. Strey and T. Schmeling, *Berichte der Bunsengesellschaft für physikalische Chemie*, 1983, **87**, 324–327.

6 C. M. Phan, T. N. Le, C. V. Nguyen and S.-i. Yusa, *Langmuir*, 2013, **29**, 4743–4749.

7 C. M. Phan, C. V. Nguyen and T. T. T. Pham, *The Journal of Physical Chemistry B*, 2016, **120**, 3914–3919.

8 C. Vega and E. de Miguel, *The Journal of Chemical Physics*, 2007, **126**, 154707.

9 J. Alejandre and G. A. Chapela, *The Journal of Chemical Physics*, 2010, **132**, 014701.

10 M.-M. Walz, C. Caleman, J. Werner, V. Ekholm, D. Lundberg, N. L. Prisle, G. Öhrwall and O. Björneholm, *Physical Chemistry Chemical Physics*, 2015, **17**, 14036–14044.

11 M.-T. Lee, F. Orlando, L. Artiglia, S. Chen and M. Ammann, *The Journal of Physical Chemistry A*, 2016, **120**, 9749–9758.

12 J. Gliński, G. Chavepeyer, J.-K. Platten and P. Smet, *The Journal of Chemical Physics*, 1998, **109**, 5050–5053.

13 S. Pezzotti, D. R. Galimberti, Y. R. Shen and M.-P. Gaigeot, *Physical chemistry chemical physics: PCCP*, 2018, **20**, 5190–5199.

14 S. Lenton, N. H. Rhys, J. J. Towey, A. K. Soper and L. Dougan, *The Journal of Physical Chemistry B*, 2018, **122**, 7884–7894.

15 F. Biscay, A. Ghoufi and P. Malfreyt, *The Journal of Chemical Physics*, 2011, **134**, 044709.